Targeted Prostate Biopsy Using Statistical Image Analysis

Yiqiang Zhan*, Dinggang Shen, *Senior Member, IEEE*, Jianchao Zeng, Leon Sun, Gabor Fichtinger, *Member, IEEE*, Judd Moul, and Christos Davatzikos, *Senior Member, IEEE*

***Abstract*—In this paper, a method for maximizing the probability of prostate cancer detection via biopsy is presented, by combining image analysis and optimization techniques. This method consists of three major steps. First, a statistical atlas of the spatial distribution of prostate cancer is constructed from histological images obtained from radical prostatectomy specimen. Second, a probabilistic optimization framework is employed to optimize the biopsy strategy, so that the probability of cancer detection is maximized under needle placement uncertainties. Finally, the optimized biopsy strategy generated in the atlas space is mapped to a specific patient space using an automated segmentation and elastic registration method. Cross-validation experiments showed that the predictive power of the optimized biopsy strategy for cancer detection reached the 94%–96% levels for 6–7 biopsy cores, which is significantly better than standard random-systematic biopsy protocols, thereby encouraging further investigation of optimized biopsy strategies in prospective clinical studies.**

***Index Terms*—Biopsy optimization, prostate cancer, spatial normalization, statistical image analysis.**

I. Introduction

With an aging population, prostate cancer has become a major medical and socioeconomic problem. It continues to be the second leading cancer death course for American men. Since prostate cancer is relatively less aggressive and slowly progressing, if the cancer can be found while it is still confined in the prostate, the 5-year relative survival rate after the treatment is nearly 100% [1]. Therefore, early diagnosis is critically important for treating prostate cancer. In the absence of an imaging modality that can reliably detect prostate cancer in the majority of cases, needle biopsy of the prostate following an elevated prostate specific antigen (PSA) levels or an abnormal digital rectal examination (DRE) has been widely used as a gold standard for the diagnosis of prostate cancer. The most popular sampling method has been the sextant biopsy [2], which divides the left and right parts of the prostate into three regions each, then randomly samples each of them. This approach has been shown to have a large false negative detection rate ranging from 27% to 39%, depending on cancer stage [3], [4]. For example, the study in [5] showed that 23% of initially positive sextant biopsies were followed by a negative repeat biopsy, indicating the significant error of the technique. Similar data have been published by others showing 31% [6] and 23% [7] negative repeat sextant biopsy of patients with positive first biopsy. Enhanced biopsy methods have also been employed, with the number of needles varying from 8 to 14, or, in the case of saturation biopsy, up to 45 core needle samples [8]–[14], generally displaying improved detection rates. However, each additional puncture on the rectal wall increases the possibility of infection and makes the patients more uncomfortable even when the biopsy is performed under local anaesthesia.

The low predictive accuracy of the random systematic biopsy strategies is partly due to their highly empirical nature, i.e., the needles are just randomly deployed without considering the fact that the spatial distribution of prostate cancer is inhomogeneous within the prostate capsule [15], [16]. Recently, some researchers have begun to investigate the possibility of using a large number of patients' histological images to determine prostate regions that are most likely to develop cancer and therefore should be sampled during biopsy [17]–[19]. Although these methods indicate a promising direction for increasing the biopsy efficiency, they have used relatively simple spatial normalization methods, which limit the accuracy of the derived statistical distribution of caner and hence the diagnosis accuracy of biopsy.

In this paper, we propose a method that precisely determines where the needles should be placed, in order to maximize the probability of cancer detection, by applying a statistical image analysis methodology to a set of histological images obtained from radical prostatectomy patients. Our premise is that better registration methods allow us to perform more accurate voxel-based analysis of the spatial distribution of prostate cancer, which leads to a more spatially specific biopsy optimization. Our method consists of three steps. First, labeled histological images from many patients are registered to a canonical coordinate system using an elastic registration method. This canonical coordinate system is defined as *stereotactic space*, in which the same spatial coordinates correspond

Manuscript received September 20, 2006; revised December 4, 2006. This work was supported in part by the National Institutes of Health (NIH) under Grant R01 CA104976. *Asterisk indicates corresponding author.*

*Y. Zhan is with the Section of Biomedical Image Analysis, Department of Radiology, University of Pennsylvania, Philadelphia, PA 19104 USA. He is also with the Center of Computer-Integrated Surgery and the Department of Computer Science, Johns Hopkins University, Baltimore, MD 21218 USA (e-mail: yzhan@cs.jhu.edu).

D. Shen and C. Davatzikos are with the Section of Biomedical Image Analysis, Department of Radiology, University of Pennsylvania, Philadelphia, PA 19104 USA. They are also with the Center of Computer-Integrated Surgery, Johns Hopkins University, Baltimore, MD 21218 USA.

J. Zeng is with the Department of Electrical and Computer Engineering, Howard University, Washington DC 20059 USA.

L. Sun and J. Moul are with the Division of Urologic Surgery, Duke University Medical Center, Durham, NC 27710 USA.

G. Fichtinger is with the Center of Computer-Integrated Surgery and the Department of Computer Science, Johns Hopkins University, Baltimore, MD 21218 USA.

Color versions of one or more of the figures in this paper are available online at http://ieeexplore.ieee.org.

Digital Object Identifier 10.1109/TMI.2006.891497

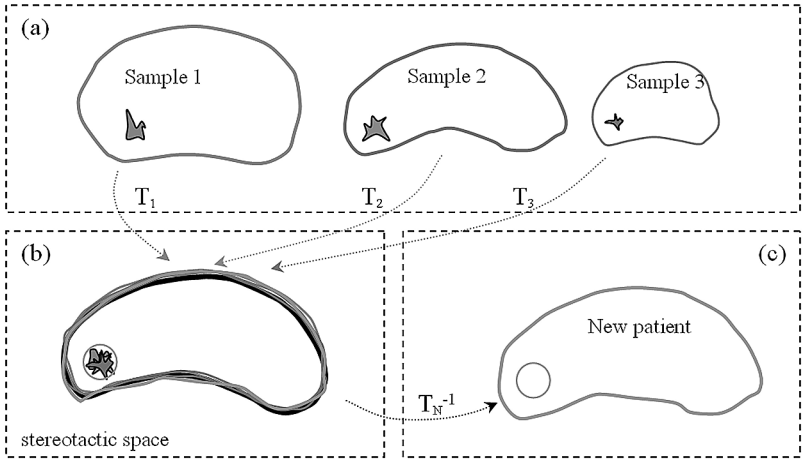

Fig. 1. Schematic demonstration of the proposed method for the optimization of the biopsy strategy. (a) The atlas is constructed from a number of histological images that are spatially normalized to the stereotactic space (the spatial normalization transformations are represented by dotted arrows). (b) Optimal biopsy sites are determined in the stereotactic space, as indicated by the black circle, based on the statistics of cancer distribution. (c) The optimal biopsy site is then mapped back to the patient's image space via the transformation $\mathrm{T}_{\mathrm{N}}^{-1}$.

to approximately the same anatomic location in different patients. Thereby, a statistical atlas of the spatial distribution of prostate cancer is readily constructed in the stereotactic space. Second, based on the statistical atlas of the spatial distribution of prostate cancer, an optimization framework is used to deploy the biopsy needle cores, which are modeled as semi-cylinders. This optimization framework maximizes the probability that at least one needle intersects cancerous tissue under the presence of needle placement uncertainties. Finally, a method for mapping the optimized biopsy strategy to a new patient's scan for biopsy purposes is proposed. Since ultrasound imaging is commonly used for biopsy guidance in clinical settings, a texture-based segmentation method is used to determine the prostate surface from the ultrasound image and guide the deformable registration with the atlas. Fig. 1 gives a schematic example to explain the principle of our atlas-based biopsy optimization method. Notably, although theoretically it is better to optimize the biopsy cores in the patient space after warping the statistical atlas to a specific patient, the huge time cost of the atlas warping and the biopsy optimization is not affordable for real biopsy operations. Using our proposed method, the optimization of biopsy cores in the stereotactic space is accomplished before biopsy operations and the warping of the optimized biopsy strategy could be finished very fast, which satisfies the requirement of real clinical applications.

This study follows the direction of our previous work [20], which proposed to optimize biopsy strategy based on a statistical atlas of spatial distribution of prostate cancer. It is worth noting there are three major extensions in this study. First, we considered many clinically relevant factors in the optimization framework. For instance, instead of using a spherical core model, the shape of biopsy core is modeled as a semi-cylindrical model which is the same as the real biopsy needle. Also, the needle placement uncertainty, which is important from a clinical perspective, has been factored into our optimization via random displacement of the needles. Our optimization is therefore robust to such errors. Different physical constraints are also considered. These are important since a theoretically optimal plan might not be feasible in practice. Second, in order to map the optimized biopsy strategy to a specific patient using the surface-based registration method, an automatic segmentation method is designed to define the prostate capsule from ultrasound images. Finally, we stratified our database according to race, age and PSA level. Similar patterns of prostate cancer distribution are found in these subgroups and the optimized biopsy strategy exhibits consistent diagnosis accuracy across them. Compared to [20], we used a similar method to construct the statistical atlas. However, the atlas-based biopsy optimization framework in this study is substantially different from that of [20] and the application of the optimized biopsy strategy to a specific patient is a completely new part. These two parts will be described in detail in this paper.

The remainder of this paper is organized as follows. The three steps of our method will be detailed in Section II. In Section III, a set of experiments are presented to show the performance of our method in optimizing the biopsy strategy. The paper is concluded in Section IV.

II. Methods

A. Construction of the Statistical Atlas

Data Acquisition: In our study, 158 prostatectomy specimens from the tissue bank of the Center for Prostate Disease Research (CPDR) (http://www.cpdr.org) were used to construct the statistical atlas of the prostate cancer distribution. These specimens were whole mounted and step-sliced at 2.25-mm intervals. Several sections, each 5 μm thick, were prepared from every specimen, and stained with haematoxylin and eosin. The specimens were pathologically reviewed for tumors, scanned into the equipment with 3-D reconstruction software, and labeled for cancer and normal anatomy.

Spatial Normalization: Only after all the prostate subjects are normalized to a canonical coordinate system where the same coordinates approximately correspond to the same anatomic structures in different patients, could the statistical atlas of prostate cancer distribution be reliably constructed by superposing all of the normalized subjects. In our study, such a canonical coordinate system is defined as *stereotactic space*. Although volumetric registration methods [21]–[23] usually provide more so-

phisticated spatial normalization, the lack of common anatomical landmarks in the interior of the prostate precludes us to use these methods. In our study, the histology images are spatially normalized by a surface-based elastic registration method detailed next.

The 3-D surfaces of a prostate's outer capsule are first reconstructed using deformable modeling techniques [24]. One of the prostates is randomly selected as the model. In the second step, an approximate anatomical correspondence between the surface of the model prostate and all other prostates is established using [25] by matching the geometric features of the surfaces. The geometric features are designed in a multiscale fashion. In this way, different parts of prostate surfaces can be well differentiated and matched, though prostates usually have a globally symmetric shape. Finally, surface correspondence is interpolated to the interior of the prostate using a high-dimensional elastic transformation [26], which models prostates as elastic objects following mechanical equilibrium equations. In this way, the prelabeled cancerous regions are carried by the dense deformation field to the stereotactic space in which the model prostate resides. The statistical atlas of the prostate cancer distribution is then obtained by simply superposing all these normalized subjects. It is worth noting that the statistical atlas includes not only the cancer incidence at individual locations but also more general multivariant relations between different zones. These will be exploited in the following atlas-based biopsy optimization, so that sampling a prostate region whose cancer statistics are highly correlated with those of an already sampled location is to be avoided, in general.

B. Atlas-Based Biopsy Optimization

Optimization Framework: Based on the statistical atlas constructed by a set of spatially normalized histological datasets, a K-needle biopsy strategy is optimized to maximize the probability that at least one needle intersects cancerous tissue. Conversely, the probability that none of the K needles intersects cancerous tissue is minimized.

Fig. 2(a) shows an example of the biopsy needle, which consists of the outer core and the inner stylet that has a "cut-out" [27]. When the inner stylet is inserted into the position where the tissue is supposed to be extracted, a piece of tissue settles into the cut-out. Almost instantaneously, the outer core moves forward and cuts off the piece of tissue that has settled into the cut-out of the inner stylet. As the bottom of the cut-out is a plane, the biopsy core can be modeled as a semi-cylindrical volume, whose position can be exclusively determined by three parameters [c.f. Fig. 2(b)], i.e., $\vec{c}$, the center of the bottom plane of the semi-cylindrical cut-out, $\vec{l}$, the orientation of the semi-cylindrical cut-out, and $\vec{r}$, the orientation perpendicular to the bottom of the cut-out. For a K-needle biopsy strategy, the optimization problem can be summarized as determining the position parameters of each biopsy cut-out so that the probability that no cancerous tissue is included in the K semi-cylinders is minimized. Mathematically, it can be represented as

$$\min_{\vec{t}_1,\cdots,\vec{t}_K} P\left(B(\vec{t}_1)=\mathrm{NC},\cdots,B(\vec{t}_K)=\mathrm{NC}\right) \quad (1)$$

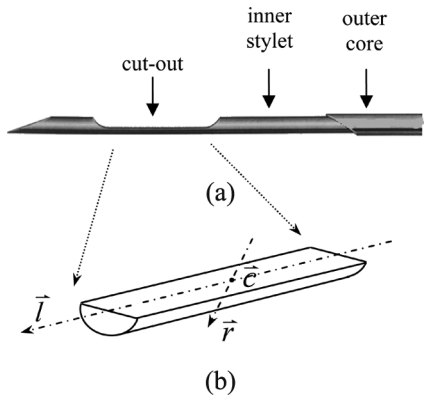

Fig. 2. Schematic diagram of the biopsy needle model used in our experiments. (a) The profile of a biopsy needle. (b) The semi-cylindrical model of the biopsy core. The three position parameters are $\vec{c}$, the center of the bottom plane of the semi-cylindrical cut-out, $\vec{l}$, the orientation of the semi-cylinder cut-out, and $\vec{r}$, the orientation perpendicular to the bottom of the cut-out.

where $\vec{t}_i$ is a vector consists of the three position parameters $\vec{c}_i$, $\vec{l}_i$ and $\vec{r}_i$ of the ith needle. $B(\vec{t}_i)$ is the biopsy outcome of the ith needle, and NC denotes a negative cancer detection result.

As (1) is a high dimensional optimization problem with many local minima, we use simulated annealing to solve it. This optimization method starts with an initial guess for the position parameters of the K needles, and then iteratively changes all position parameters towards a direction that decreases the probability function in (1), while randomly allowing steps in the opposite direction, as customary in random optimization methods aiming at avoiding local minima. Since simulated annealing is successful and practical only if a good initial guess of the desired optimal solution is somehow determined, we designed a fast heuristic method for determining a good initial guess of the position parameters of the K needles, which is detailed next.

A Fast Heuristic Method for Initial Optimization: The goal here is to place the needles in the regions where cancer incidence is high, and which are statistically independent of each other. Following this idea, (1) is expressed as a product of conditional probabilities

$$\begin{aligned} &P\left(B(\vec{t}_i)=\mathrm{NC}, i=1,\cdots,K\right) \\ &\quad = P\left(B(\vec{t}_1)=\mathrm{NC}\right) \times P\left(B(\vec{t}_2)=\mathrm{NC}|B(\vec{t}_1)=\mathrm{NC}\right) \times \cdots \\ &\qquad \times P\left(B(\vec{t}_K)=\mathrm{NC}|B(\vec{t}_i)=\mathrm{NC}, \mathrm{i}=1,\cdots,\mathrm{K}-1\right). \end{aligned} \quad (2)$$

Suppose that there are M prostate subjects in the training set. To minimize (2), the first biopsy needle is placed in the position with the parameters $\vec{t}_1$, where the cancer incidence of the M subjects is the highest, i.e., $P(B(\vec{t}_1)=\mathrm{NC})$ is the lowest. Knowing the parameters of the first biopsy, the conditional probability $P(B(\vec{t}_2)=\mathrm{NC}|B(\vec{t}_1)=\mathrm{NC})$ is calculated by excluding those prostate subjects whose cancer has been detected by the first needle, since they do not satisfy the condition $B(\vec{t}_1)=\mathrm{NC}$. Importantly, if the incidence of cancer at a location is strongly related with the incidence of cancer in the region included by the first biopsy needle, the cancer occurrence probability of this location will become very low when conditioned by $B(\vec{t}_1)=\mathrm{NC}$. This implies that the second biopsy will most likely be placed in regions that display cancer incidence independent of that in the region of the first biopsy needle. With this new conditional probability, $\vec{t}_2$, the position parameters of the second needle can

be determined by minimizing the conditional probability. Using the same procedure, the position parameters of other biopsy needles $\vec{t}_3, \cdots, \vec{t}_K$ are sequentially determined.

The remaining problem is how to determine the position parameters of a single biopsy needle given the conditional probability map. For instance, to determine the position parameters of the jth needle, we need to minimize the multivariant conditional probability $P(B(\vec{t}_j) = \mathrm{NC} | B(\vec{t}_i) = \mathrm{NC}, \mathrm{i} = 1, \cdots, j-1)$, in which $\vec{t}_j$ consists of three position parameters $\vec{c}_j, \vec{l}_j$ and $\vec{r}_j$. We use a heuristic optimization method to sequentially optimizes these three parameters that denote the center and the orientations of the needle. The result of this sequential optimization method is used as an initial guess for the position parameters of the K needles, and then the simulated annealing technique is used to find globally optimal solutions for $\vec{t}_1, \cdots, \vec{t}_K$.

Robustness to Needle Placement Error: In a real biopsy procedure, needle placement is subject to error and uncertainties. Therefore, we incorporated a random perturbation procedure into our optimization framework, in order to make the optimized biopsy strategy robust to needle placement errors. Our basic idea is that the optimized biopsy strategy should maximize the cancer detection rate while allowing the needles to be randomly perturbed within a range that relates to needle placement accuracy. Assume that $\vec{t}_{i,1} \ldots \vec{t}_{i,P}$ is a set of random perturbations of $\vec{t}_i$, i.e., the position parameters of the ith needle. As long as the cancer can't be detected by *all* these perturbed needle positions, it is regarded as being missed by the ith needle in the optimization framework. Accordingly, the probability function in (1) is reformulated by replacing $B(\vec{t}_i) = \mathrm{NC}$ with $\hat{B}(\vec{t}_i) = \mathrm{NC}$, which is defined as

$$\left\{\hat{B}(\vec{t}_i) = \mathrm{NC}\right\} \equiv \left\{B(\vec{t}_{i,1}) = \mathrm{NC} \| B(\vec{t}_{i,2}) = \mathrm{NC} \| \cdots \| B(\vec{t}_{i,P}) = \mathrm{NC}\right\} \quad (3)$$

where P is the number of random perturbation cases considered. Note that this is a very strict definition, which requires that, for a tentative needle configuration, if cancer is detected, cancer is also present in the vicinity of the needles.

The following strategy is added in our optimization framework to optimize the reformulated objective function. After the position parameters of a single biopsy needle are determined by minimizing its corresponding conditional probability, this needle is randomly shifted to several positions in a small neighborhood, i.e., the position parameters of the needle are perturbed within a small range. In this paper, the center of the needle is shifted in a sphere with 4-mm diameter, which is determined according to the needle placement error (around 2.0 mm) of a robotic biopsy system designed by our collaborators [28]. Only the prostate subjects whose cancerous tissues are detected by *all* of the randomly shifted needles are considered as a positive sample and are therefore excluded from the dataset for recalculating the conditional probability.

Physical Constraints: Up to now, we have assumed that an optimized needle placement can be implemented in any real clinical setting. However, different clinical settings actually have different physical constraints. In our study, we considered two mostly used biopsy approaches, i.e., trans-perineal biopsy and trans-rectal biopsy. The former type of biopsy tends to constrain the orientation of the needles along the base-apex direction, whereas the latter constrains it to be along the anterior-posterior direction.

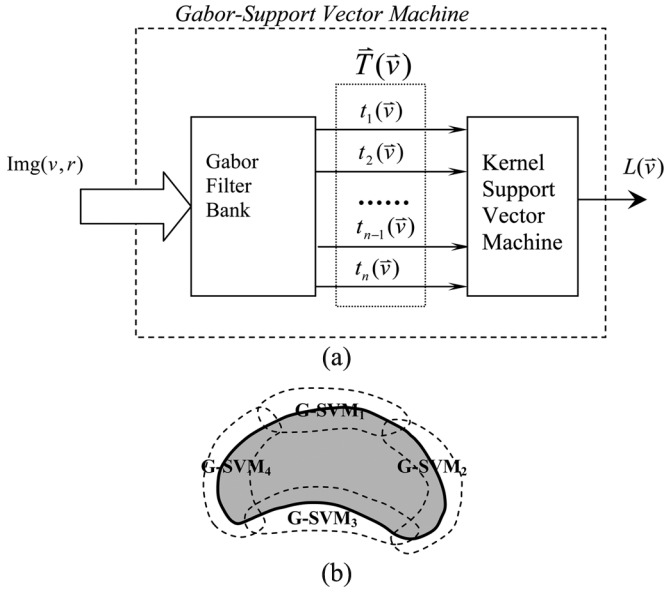

Fig. 3. Schematic description of G-SVM used in automatic prostate segmentation. (a) The structure of a single G-SVM, which consists of a Gabor filter bank and a kernel SVM. Given a r × r × r subimage, $\mathrm{Img}(\vec{v}, r)$, with the center at voxel $\vec{v}$, the Gabor filter bank extracts the Gabor texture features around voxel $\vec{v}$, i.e., $\vec{T}(\vec{v}) = [t_1(\vec{v}), \cdots, t_n(\vec{v})]^T$. These texture features $\vec{T}(\vec{v})$ are input to a pretrained kernel SVM for generating a texture label, $L(\vec{v})$, indicating the likelihood of $\vec{v}$ belonging to the prostate tissue. (b) Schematic description of the spatially distributed G-SVMs. The model surface (thick solid contour) is divided into four subsurfaces, and their corresponding G-SVMs are trained by the samples selected from their neighboring regions (regions surrounded by the dashed curves), respectively.

C. Application of the Optimized Biopsy Strategy

Surface-Based Registration With Automatic Ultrasound Image Segmentation: The optimized biopsy strategy generated in the stereotactic space must be mapped to the patient space for a real application. For consistency, the registration method used for constructing the statistical atlas is also employed to register the atlas with the patient's scan. Since this registration method is surface-based, it is necessary to extract the patient's prostate capsule surface from the scan. Considering that ultrasound imaging is a generally used imaging device in the biopsy operations, we designed a method to automatically delineate the prostate capsule surface from 3-D ultrasound images [29].

We use a 3-D deformable model [30] which does not employ edge information but relies on texture characteristics to delineate prostate boundaries, because ultrasound images usually have a low signal-noise-ratio but have abundant texture information. In particular, Gabor-support vector machines (G-SVMs) are designed to capture texture priors of ultrasound images and differentiate prostate and nonprostate tissues by statistically analyzing their textures. Shown in Fig. 3(a), each G-SVM consists of a *Gabor filter bank* for extraction of rotation-invariant texture features and a *kernel support vector machine* for robust differentiation of textures. Due to its multiscale and multiorientation structure, the Gabor filter bank is able to extract rich texture features from noisy ultrasound images. Also, as the Gabor filter incorporates Gaussian smoothing, it is robust to image noise.

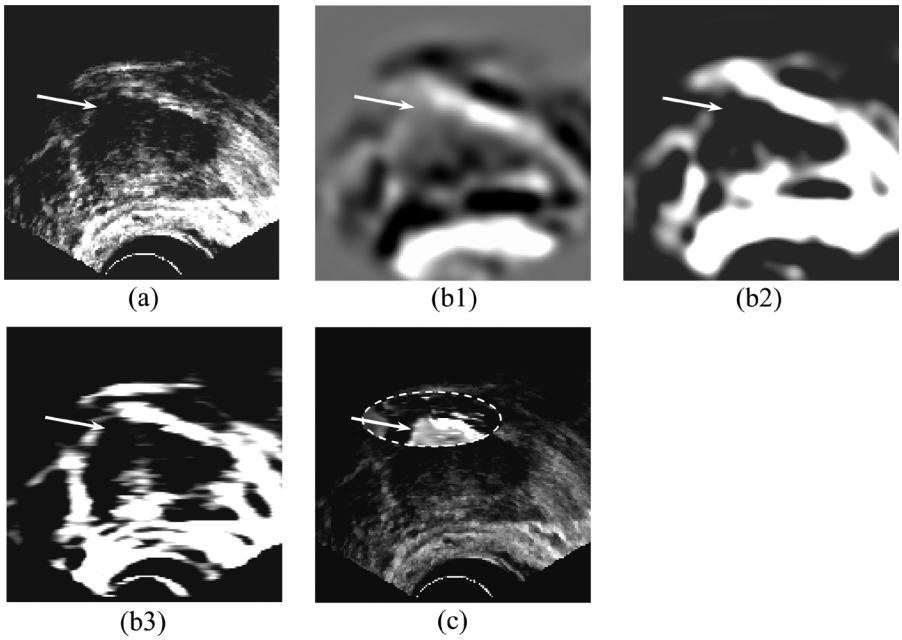

Fig. 4. The performance of our texture analysis method (G-SVM) in differentiating the prostate boundary. (a) A typical TRUS image obtained from the top section of the prostate; an example of a region in which the prostate boundary is unclear is indicated by white arrow; (b1–b3) three Gabor feature maps computed from (a); (c) tissue differentiation results using a pretrained G-SVM, where the labeling results are shown in an ellipsoidal region for comparison. For display purposes, labeling results, which originally range from 0 to 1, have been mapped to 0∼255.

The kernel SVM (KSVM) is selected to label tissues based on texture features because it is able to nonlinearly separate different classes in a high dimensional space with maximum generalization ability. By employing both Gabor filter banks and KSVM, a pretrained G-SVM is robust in differentiating tissues in *a local region*. Fig. 4(a) shows an example of the not easily defined prostate boundary in an ultrasound image. In Fig. 4(c), the tissues around the prostate boundaries are efficiently labeled by a pretrained G-SVM, even though they are not differentiable either in the original image [c.f. Fig. 4(a)] or in any individual Gabor feature map [c.f. Fig. 4(b1)–(b3)].

Considering that the same prostate tissue may have very different texture features along the prostate boundary in ultrasound images, it is difficult to use a single G-SVM to correctly label all prostate tissues in the images. Therefore, we use a number of G-SVMs, each of which is attached to a subsurface of the deformable model, in order to adaptively label tissues around the prostate boundary. Particularly, subsurfaces are uniformly divided from the entire deformable surface model, and they are designed to be overlapped with each other [c.f. Fig. 3(b)]. In the training stage, each G-SVM is only trained by the samples extracted from the neighborhood of its corresponding subsurface. In the segmentation stage, each G-SVM is only in charge of tissue differentiation in the neighborhood of its corresponding subsurface as well. As the texture features of tissues around a specific subsurface usually exhibit relatively simple distribution in the feature space, multiple G-SVMs provide more robust tissue differentiation results.

Given the prostate ultrasound image of a specific patient, the initial position of the deformable model is determined by transforming it to a pose which optimally matches with prostate boundary in the ultrasound image. In particular, a set of robust features captured by Gabor filter banks are selected to evaluate the matching degree. Then the pretrained G-SVMs are employed to tentatively label the voxels in the neighborhood of the initial model surface. Subsequently, the surface of the deformable model is deformed to the boundary between the tentatively labeled prostate and nonprostate tissues. The step of tissue labeling and the step of label-based surface deformation are iterated until the model surface converges to the prostate boundaries. The converged model is regarded as the prostate surface of the specific patient extracted from the ultrasound image. Then the correspondences between the atlas prostate capsule surface and the patient's prostate capsule surface are established using the method in [25] and interpolated to the interior of the prostate using elastic warping [26]. In this way, the optimized biopsy strategy is adapted to the specific patient for a real biopsy operation.

Linearization of Warped Biopsy Cores: Since the optimized biopsy strategy are mapped to the patient space using an elastic model [26], the shapes of biopsy cores are unavoidably warped and are no longer semi-cylinders. Therefore, the mapped biopsy cores are further linearized to be applied to a real biopsy operation. In this paper, principal component analysis (PCA) is first employed to find the three principal axes of the warped biopsy cores. The axis with the largest eigenvalue is regarded as $\vec{l}$, i.e., the orientation of the biopsy core, and the axis with the smallest eigenvalue is regarded as $\vec{r}$, i.e., the orientation perpendicular to the bottom of the cut-out. Using the center of the warped biopsy core as $\vec{c}$, along with the $\vec{l}$ and $\vec{r}$ obtained via PCA, a semi-cylindrical model can be constructed. The three position parameters are further adjusted within a small range so that the linearized semi-cylindrical model has the maximum overlap with the warped biopsy cores. In this way, the linearization has very limited influence to the predictive accuracy of the optimized biopsy strategy.

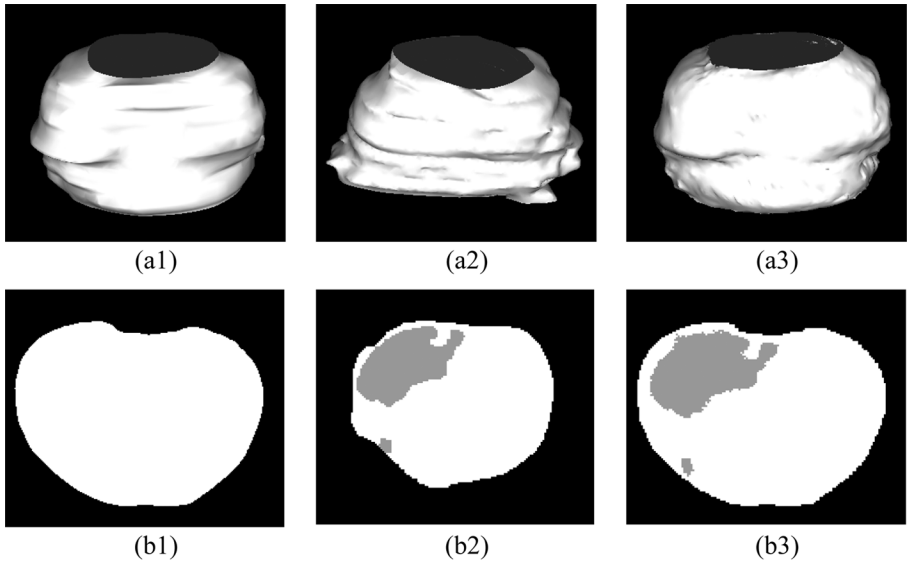

Fig. 5. An example of the spatial normalization of a prostate subject. (a1) Three-dimensional rendering of the model prostate. (a2)–(a3) Three-dimensional renderings of a prostate subject before and after the elastic registration. The white surface denotes the outer capsule of the prostate. (b1) A cross section of the model prostate. (b2–b3) A cross section of the prostate with labeled cancer region before and after the spatial normalization. The labeled cancer regions are denoted as grey regions.

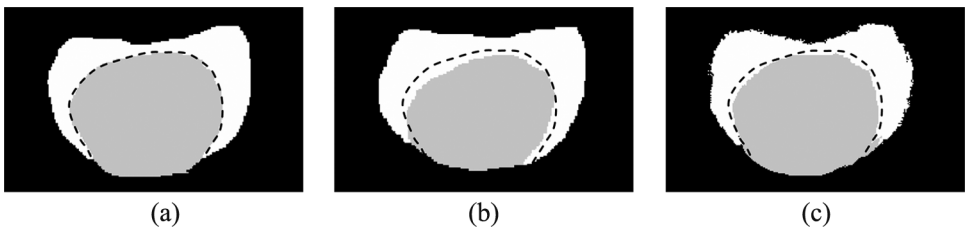

Fig. 6. An example to verify that the spatial normalization method preserves prostates' zonal geometry. The grey and the white regions denote the central zone and the peripheral zone, respectively. (a) subject 1, (b) subject 2, (c) warped subject 2 using our surface-based registration method. The dashed line, used as reference, is the boundary between the central zone and the peripheral zone of subject 1.

III. Experiments

In this section, we present a set of experiments to validate the performances of our method in optimizing the biopsy strategy. The experiments are divided into three groups, corresponding to the three steps of our method, i.e., the construction of statistical atlas, the atlas-based biopsy strategy optimization, and the application of the optimized biopsy strategy.

A. Construction of the Statistical Atlas

The first set of experiments relate to the construction of the statistical atlas using the proposed spatial normalization method. Fig. 5 shows a representative example of the spatial normalization of a prostate subject. Fig. 5(a1) shows the 3-D rendering of the model surface. Fig. 5(a2)–(a3) shows the 3-D renderings of the subject surface before and after the elastic registration. Comparing Fig. 5(a1) and (a3), the registered subject surface is very similar to the model though they have large shape difference before registration [c.f. Fig. 5(a2)]. Fig. 5(b1) shows a cross section of the model. Fig. 5(b2)–(b3) show the same cross section of the subject with cancerous regions labeled before and after the spatial normalization. In this way, the prelabeled cancerous regions are carried by the dense deformation field to the stereotactic space in which the model prostate resides.

Since prostate cancer distribution is strongly affected by the geometry of the prostate zones, it is important to verify if the spatial normalization distorts the zonal geometry. Therefore, we use the proposed surface-based registration method to register two prostate subjects whose peripheral zones were manually labeled. As shown in Fig. 6, the peripheral zones of the registered subjects are largely overlapped with the overlap volume error 16.5%. Compared to the affine registration method that produces the overlap volume error 34.4%, the proposed normalization method exhibits much better performance in preserving the zonal geometry of prostates.

After the spatial normalization of all the prostate subjects, the statistical atlas of the prostate cancer distribution is obtained by superposing all these warped prostate subjects with their labeled cancerous regions. The top-left image in Fig. 7 shows the statistical atlas constructed by 158 prostate subjects from the CPDR database. We manually labeled the peripheral zone in the model space and found that 72.2% warped prostate subjects have cancerous tissues in the peripheral zone. This result is in agreement with the general clinical assumption that 70%–80% prostate cancers form in the peripheral zone, which again proves

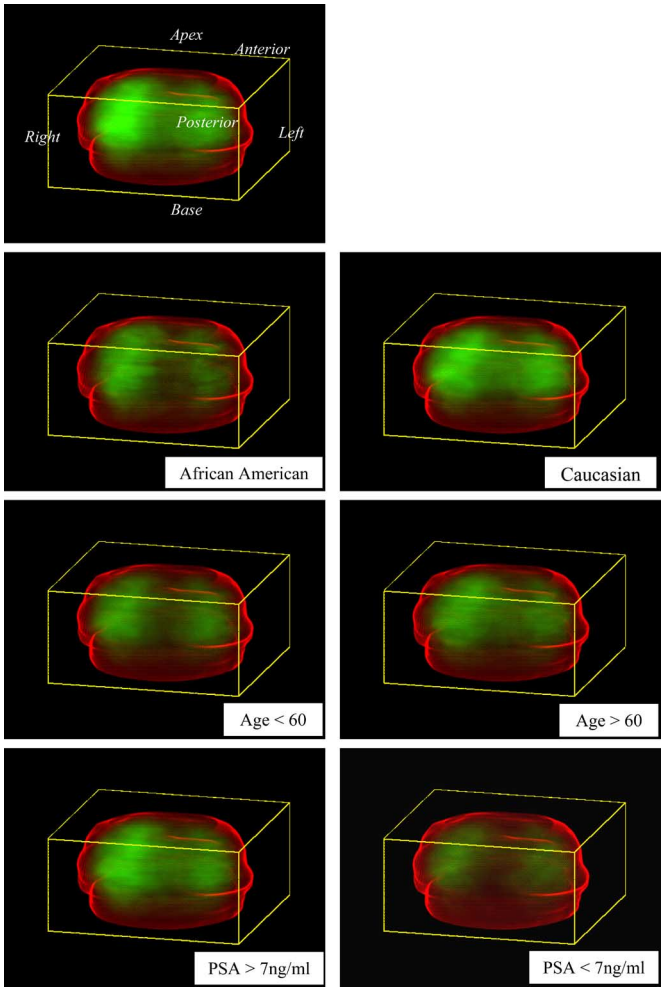

Fig. 7. Statistical atlases of the spatial distribution of prostate cancer. The red contour is the 3-D rendering of the surface of the model prostate capsule. The green region represents the frequency of prostate cancer occurrence. Brighter green indicates higher probability of the cancer occurrence in that location. The top-left image shows the statistical atlas constructed by all of the 158 prostate subjects. The bottom three rows show the statistical atlases constructed by categorized subjects based on race (African American versus Caucasian), age ($<$60 versus $>$60) and PSA level ($>$7 ng/ml versus $<$7 ng/ml), respectively.

that our spatial normalization method is good at preserving the zonal geometry of prostates.

Considering the spatial statistics of cancer distribution might be different across patient groups with significant demographic or clinical differences, we further partition the 158 subjects into different subgroups according to race, i.e., African American (38) versus Caucasian (102), age, i.e., $\mathrm{age} > 60$ (78) versus $\mathrm{age} < 60$ (64), or PSA level, i.e., $\mathrm{PSA} > 7\ \mathrm{ng/ml}$ (70) versus $\mathrm{PSA} < 7\ \mathrm{ng/ml}$ (67) (The number in the parenthesis denotes the number of samples in the subgroup). The statistical atlases of cancer distribution corresponding to different subgroups are shown in Fig. 7. It is worth noting that, although the distributions of prostate cancer are different in those statistical atlases, they share many common characteristics, e.g., the prostate cancer has higher incidence in peripheral zones and the mid and the apical zones exhibit higher cancer incidence than the base zones, all of which are in agreement with what is known from clinical studies [31].

B. Atlas-Based Biopsy Optimization

In the second set of experiments, we validated the predictive power of our atlas-based optimized biopsy strategy. Fig. 8 summarizes the optimization results for the semi-cylindrical biopsy core model. In Figs. 8(a)–(c), 3-D renderings of the model prostate capsule (red) and the spatial distribution of cancer occurrence (green), along with the six optimal biopsy cores (white) are shown.

We used the leave-one-out method to validate the predictive power of the optimized biopsy strategy. For each time, we selected one subject from our 158 prostate subjects, and the statistical atlas was regenerated from the remaining 157 subjects. The optimized biopsy strategy based on this atlas was applied to the left-out subject. We repeated this procedure 158 times to measure the probability of missing the cancer using our optimized biopsy strategy. Each semi-cylindrical biopsy core in this experiment has the length 12.7 mm and the radius 0.8 mm, which is the same as a widely used biopsy needle [32]. Fig. 8(d) plots the detection rate as a function of the number of biopsy cores. For six needles, our optimized biopsy strategy could achieve the cancer detection rate of 96.2%. Compared to the simulated standard sextant biopsy on the same dataset, which yielded detection rate of 70.5%, our biopsy strategy has much higher diagnosis accuracy. For more comparisons, we also tested Zeng's method [24] on the same dataset. Since that method used a rough registration method for atlas construction, the biopsy locations could be only optimized on a resolution of prostate zones. That method had a detection rate 79.3% using six needles and 82.9% using 8 needles. The better performance of our proposed method shows the importance of using a precise registration for spatial normalization and a voxel-wise biopsy optimization. Fig. 8(d) also shows the results obtained after incorporating the random perturbations accounting for needle placement errors. The experimental results show the cancer detection rates are only slightly lowered under the approximate placement simulation. In addition, to illustrate the consistency of the optimized biopsy strategy on patient groups with different demographic or clinical values, we applied the optimized seven-needle biopsy strategy on the subgroups described in Section III-A. Table I shows that the optimized seven-needle biopsy strategy has consistent diagnostic accuracy across different patient groups, evaluated via cross-validation.

We also tested the optimized biopsy strategy for different physical constraints, as we discussed in Section II-B. Fig. 9 shows analogous cross validation results for the optimal trans-perineal and trans-rectal biopsy cores. Since trans-perineal and trans-rectal biopsy strategies are two most popular biopsy protocols in various clinical centers, the high cancer detection rate shows the potential of using our method in real clinical implementations.

C. Warping of the Atlas to Patient Images

In the third set of experiments, we evaluated the performance of our method in applying the optimized biopsy strategy to a specific patient. Recall that the registration method for mapping the optimized biopsy strategy is the same as what is used for the spatial normalization and the atlas construction for consistency purposes. Therefore, the performance of warping of the atlas

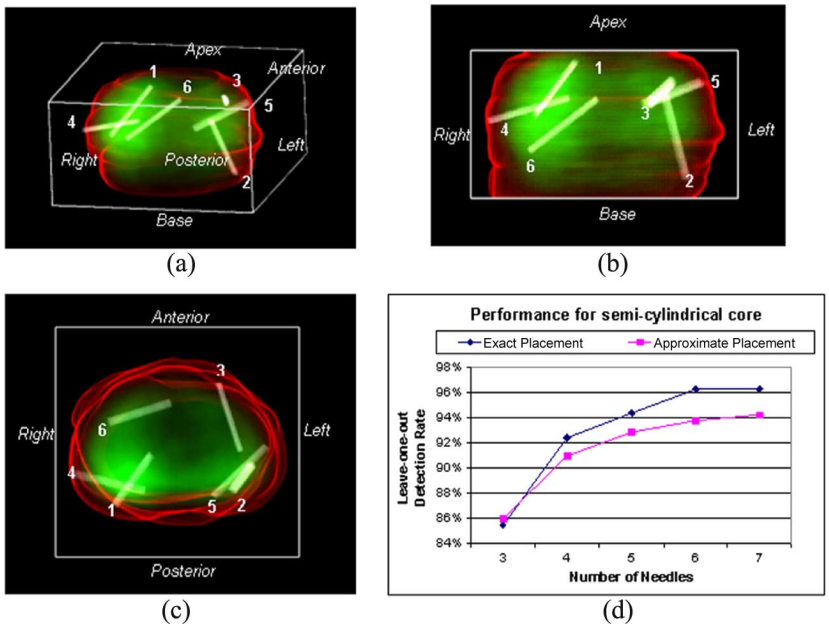

Fig. 8. Results from the semi-cylinder biopsy needle model. (a)-(c) Optimal positioning of six needles. (d) Cross-validated performance assuming exact and approximate (within a neighborhood of diameter 4 mm) needle placement.

TABLE I
CANCER DETECTION RATE OF THE OPTIMIZED SEVEN-NEEDLE BIOPSY STRATEGY ON SUBGROUPS CATEGORIZED BY RACE, AGE, AND PSA LEVEL

	Exact Needle Placement (%)	Approximate Needle Placement (%)
African American	97.2	97.1
Caucasian	94.9	92.7
Young (< 60)	95.2	91.7
Old (> 60)	95.6	94.6
Low PSA (< 7.0ng/ml)	98.4	94.2
High PSA (> 7.0ng/ml)	95.6	94.2

to the patient scans depends on the accuracy of the automatic segmentation method, which drives the elastic warping. In [29], the robustness and accuracy of our segmentation method had been extensively validated by both synthesized and real ultrasound images. Here, the method is further evaluated by applying it on atlas warping as follows. First, the prostate boundaries were delineated from patients' ultrasound images by an expert. They were also segmented by our automatic segmentation algorithm. (Since the G-SVMs in our automatic segmentation algorithm are learning-based, we used a leave-one-out mechanism to guarantee the independence between training and testing samples, i.e., each time we trained our model by all but one patient, and then used the trained model to segment prostate boundaries of the left-out patient.) Then the optimized biopsy strategy was mapped to the patient space twice based on manual and automatic segmentation results, respectively. The two mapped biopsy strategies were compared by measuring the distances of the corresponding biopsy core centers and the overlap volume error of the corresponding biopsy cores. Fig. 10 shows an example for visual comparison of the manual segmentation and automatic segmentation results. Table II presents the quantitative comparison results of six different patients. The average distance between biopsy cores is 0.43 mm and the average overlap error is 7.61%. These results show that the automatic segmentation method provides needle placement that is very comparable to the placement obtained via manual definition of the prostate capsule.

All experiments were operated on a 2.8 G Intel Xeon processor with UNIX operation system. In constructing the statistical atlas, it took about 25 min to normalize one subject onto the stereotactic space, and totally it took about 66 h for 158 subjects. Obviously, it can be implemented in a parallel way, thus reducing the processing time to around 8 h for all 158 subjects by using 8 processors. In optimizing the biopsy strategy, it took 1.5 h using one processor. It is worth noting that the large computational cost is not a serious problem for clinical applications, since both the statistical atlas construction and the atlas-based biopsy optimization are accomplished offline.

The speed for warping the optimized biopsy strategy to a specific patient is important for real clinical applications. Currently it took 15 min without code optimization. In the future, we plan to speed up the warping algorithm by optimizing software codes and using high performance hardware, e.g., Graphics Processing Unit [33].

IV. DISCUSSION AND CONCLUSION

We proposed an approach to determine the targeted biopsy needle placement in order to maximize the probability of cancer detection. We used labeled histological images of radical prostatectomy specimens to construct the statistical atlas of prostate cancer distribution. Based on the statistical atlas, an optimized biopsy strategy was generated to maximize the cancer detection rate, and to be warped onto a specific patient automatically. The cross validation experiment shows that the proposed method can achieve 94%–96% detection accuracy, which is much higher than the detection rate (70.5%) obtained on the same datasets via the commonly used sextant biopsy strategy.

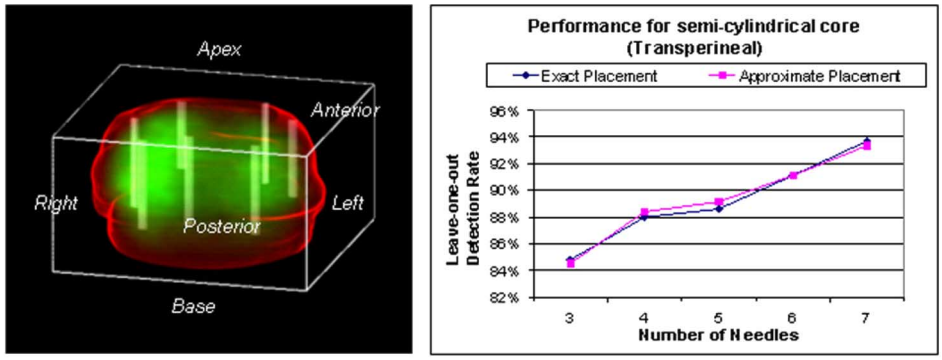

(a)

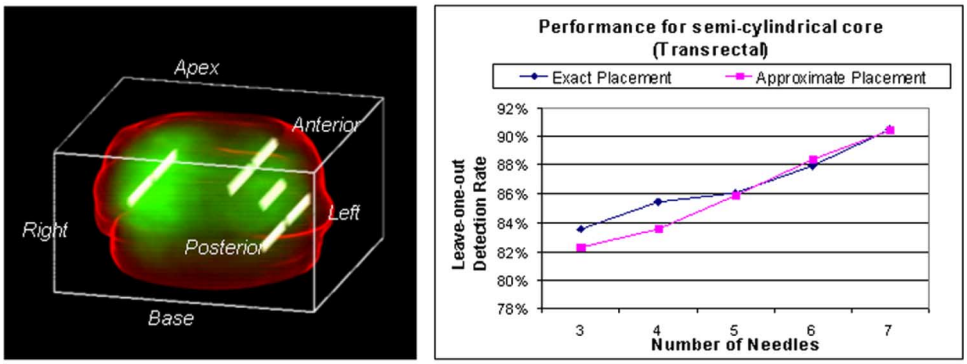

(b)

Fig. 9. (a) Optimal trans-perineal biopsy and associated detection rates via cross-validation. (b) Optimal trans-rectal biopsy and associated detection rates via cross-validation.

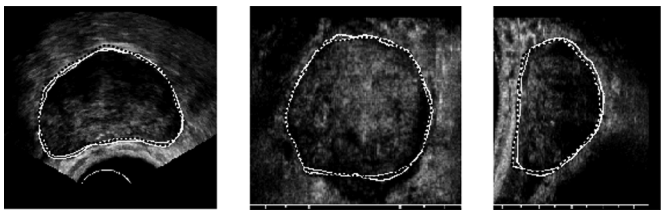

Fig. 10. Visual comparisons between algorithm-based and hand-labeled segmentation results on an ultrasound image. The white contours are the hand-labeled results, while the dashed ones are the algorithm-based segmentation results. Images from the left to the right show the axial view, coronal view and sagittal view, respectively.

TABLE II
COMPARISON OF THE BIOPSY STRATEGY BASED ON MANUAL SEGMENTATION AND AUTOMATIC SEGMENTATION

	Distance between Core Centers (mm)	Overlap Volume Error (%)
Subject1	0.24	4.91
Subject2	0.77	10.9
Subject3	0.26	6.06
Subject4	0.46	5.17
Subject5	0.26	8.24
Subject6	0.60	10.4
Mean	**0.43**	**7.61**
Stand. Deviation	**0.22**	**2.62**

A potential limitation of our study is that the spatial statistics of cancer distribution might be biased by the method used for biopsy, namely the sextant biopsy in this case, since most patients in this study were detected to have cancer via sextant biopsy. This limitation is inherent to any method attempting to estimate cancer distribution, since the true underlying distribution of cancer in a general patient population cannot be known without removing the prostates based on certain (study-specific) procedures and criteria. Future work using multiple biopsy methods can potentially remedy this bias, by including data from multiple clinical centers using different biopsy schemes. Such a multicenter study extends beyond the scope of this study.

The optimized biopsy strategy can be implemented in conjunction with 3-D ultrasound images, 3-D MRI images, or limited stacks of 2-D ultrasound images that allow for 3-D registration. Given the current direction of the clinical practice, we plan to implement the optimized biopsy strategy using a robotic system designed by our collaborators [28]. In this system, the robot is spatially registered and calibrated to the TRUS devices so that the insertion depth and orientation of the needle with respect to the stepper base [34] can be obtained from TRUS images. The robot receives each entry/target coordinate pair of the needle placement plan and inserts a preloaded needle. Experiments on phantoms showed the average placement error is around 2 mm, which is accurate enough for the implementation of our optimized biopsy strategy. In our future work, we plan to integrate our proposed method with these sophisticated robotic systems [28], [35] for accurate implementation.

The potential use of this optimization technique reaches beyond biopsy. In particular, therapeutic procedures, such as radiotherapy or gene therapy, can be adapted to population-based statistics of cancer distribution, in order to emphasize more

aggressive treatment of areas likely to develop cancer. Moreover, compared to the entire burn-out radiotherapy, the partial burn-out scheme increases "quality of life" of the patients after treatment, which is one of the hotspots of current clinical research. The further development, application and testing of this approach to diagnostic and therapeutic procedures are among our future work plans.

ACKNOWLEDGMENT

The authors would like to acknowledge the DoD Center for Prostate Disease Research for providing the histological sections.

REFERENCES

[1] [Online]. Available: http://www.cancer.orgOverview: Prostate Cancer 2006

[2] K. Hodge *et al.*, "Random systematic versus directed ultrasound guided transrectal core biopsies of the prostate," *J. Urol.*, vol. 142, no. 1, pp. 71–74, 1989, discussion 74-5.

[3] A. Manseck *et al.*, "Is systematic sextant biopsy suitable for the detection of clinically significant prostate cancer?," *Urologia Internationalis*, vol. 65, pp. 80–83, 2000.

[4] K. Fink *et al.*, "Prostate cancer detection with two sets of ten-core sextant biopsies," *Urology*, vol. 58, pp. 735–739, 2001.

[5] F. Rabbani *et al.*, "Incidence and clinical significance of false-negative sextant prostate biopsies," *J. Urol.*, vol. 159, no. 4, pp. 1247–1250, 1997.

[6] J. I. Epstein *et al.*, "Use of repeat sextant and transition zone biopsies for assessing extent of prostate cancer," *J. Urol.*, vol. 158, no. 5, pp. 1886–1890, 1997.

[7] C. G. Roehrborn, G. J. Pickens, and J. S. Sanders, "Diagnostic yield of repeated transrectal ultrasound-guided biopsies stratified by specific histopathologic diagnoses and prostate-specific antigen levels," *Urology*, vol. 47, no. 3, pp. 347–352, 1996.

[8] K. A. Iczkowski *et al.*, "Needle core length in sextant biopsy influences prostate cancer detection rate," *Urology*, vol. 59, no. 5, pp. 698–703, 2002.

[9] L. Egevad and M. Norberg, "The value of multiple core biopsies for predicting the Gleason score of prostate cancer," *BJU Int.*, vol. 88, pp. 716–721, 2001.

[10] G. Durkan *et al.*, "Improving prostate cancer detection with an extended-core transrectal ultrasonography-guided biopsy protocol," *BJU Int.*, vol. 89, no. 1, pp. 33–39, 2002.

[11] K. Roehl, J. Antenor, and W. Catalona, "Serial biopsy results in prostate cancer screening study," *J. Urol.*, vol. 167, no. 6, pp. 2435–2439, 2002.

[12] C. Stewart *et al.*, "Prostate cancer diagnosis using a saturation needle biopsy technique after previous negative sextant biopsies," *Urology*, vol. 166, no. 1, pp. 86–91, 2001.

[13] C. Chon, J. McNeal, and J. Presti, Jr., "Use of extended systematic sampling in patients with a prior negative prostate needle biopsy," *Urology*, vol. 167, no. 6, pp. 2457–2460, 2002.

[14] J. Presti *et al.*, "Extended peripheral zone biopsy schemes increase cancer detection rates and minimizes variance in prostate specific antigen and age related cancer rates: results of a community multipractice study," *J. Urol.*, vol. 169, no. 1, pp. 125–129, 2003.

[15] L. Eskew, R. Bare, and D. McCullough, "Systematic 5 region prostate biopsy is superior to sextant method for diagnosing carcinoma of the prostate," *J. Urol.*, vol. 157, no. 1, pp. 199–202, 1997.

[16] M. E. Chen *et al.*, "Comparison of prostate biopsy schemes by computer simulation," *Urology*, vol. 53, no. 5, pp. 951–960, 1999.

[17] M. Chen *et al.*, "Optimization of prostate biopsy strategy using computer based analysis," *J Urol.*, vol. 158, no. 6, pp. 2180–2181, 1997.

[18] J. Zeng, J. J. Bauer, and S. K. Mun, "Modeling and mapping of prostate cancer," *Comput. Graphics*, vol. 24, no. 5, pp. 683–694, 2000.

[19] Y. Zhu, S. Williams, and R. Zwiggelaar, "Computer technology in detection and staging of prostate carcinoma: a review," *Med. Image Anal.*, vol. 10, no. 2, pp. 178–199, 2006.

[20] D. Shen *et al.*, "Optimization of biopsy strategy by a statistical atlas of prostate cancer distribution," *Med. Image Anal.*, vol. 8, no. 2, pp. 139–150, 2004.

[21] G. E. Christensen, S. C. Joshi, and M. I. Miller, "Volumetric transformation of brain anatomy," *IEEE Trans. Med. Imag.*, vol. 16, no. 6, pp. 864–877, Dec. 1997.

[22] D. Shen and C. Davatzikos, "HAMMER: Hierarchical attribute matching mechanism for elastic registration," *IEEE Trans. Med. Imag.*, vol. 21, no. 11, pp. 1421–1439, Nov. 2002.

[23] L. Taylor *et al.*, "Three-dimensional registration of prostate images from histology and ultrasound," *Ultrasound Med. Biol.*, vol. 30, no. 2, pp. 161–168, 2004.

[24] J. Zeng *et al.*, "Distribution of prostate cancer for optimized biopsy protocols," presented at the MICCAI 2000, Pittsburgh, PA, 2000.

[25] D. G. Shen, E. Herskovits, and C. Davatzikos, "An adaptive focus statistical shape model for segmentation and shape modeling of 3D brain structures," *IEEE Trans. Med. Imag.*, vol. 20, no. 4, pp. 257–271, Apr. 2001.

[26] C. Davatzikos, "Spatial transformation and registration of brain images using elastically deformable models," *Comput. Vis. Image Understanding*, vol. 66, no. 2, pp. 207–222, 1997.

[27] M. D. Rifkin, *Ultrasound of the Prostate, Imaging in the Diagnosis and Therapy of Prostatic Disease*. Baltimore, MD: Lippincott Williams & Wilkins, 1997.

[28] C. Schneider, A. M. Okamura, and G. Fichtinger, "A robotic system for transrectal needle insertion into the prostate with integrated ultrasound," presented at the IEEE Int. Conf. Robotics and Automation, New Orleans, LA, 2004.

[29] Y. Zhan and D. Shen, "Deformable segmentation of 3D ultrasound prostate images using statistical texture matching method," *IEEE Trans. Med. Imag.*, vol. 25, no. 3, pp. 256–273, Mar. 2006.

[30] D. Terzopoulos and K. Fleischer, "Deformable models," *Visual Comput*, vol. 4, pp. 306–331, 1988.

[31] J. Bauer *et al.*, "In 3-D computer simulated prostate models lateral prostate biopsies increase the detection rate of prostate cancer," *Urology*, vol. 53, no. 5, pp. 961–967, 1999.

[32] [Online]. Available: http://www.upmccancercenters.comProstate Needle Biopsy 2006

[33] J. F. Bolz, E. Grinspun, and P. Schroder, "Sparse matrix solvers on the GPU: conjugate gradients and multigrid," *ACM Trans. Graphics*, vol. 22, no. 3, pp. 917–924, 2003.

[34] G. Fichtinger *et al.*, "Robotically assisted prostate brachytherapy with transrectal ultrasound guidance-Phantom experiments," *Brachytherapy*, vol. 5, no. 1, pp. 14–26, 2006.

[35] A. Krieger *et al.*, "Design of a novel MRI compatible manipulator for image guided prostate intervention," *IEEE Trans. Biomed. Eng.*, vol. 52, no. 2, pp. 306–313, Feb. 2005.